PROJECT REPORT IN TFY4330 NANOTOOLS

By Gina Harrington and Furkan Kaya

21.12.2016

"*Testing components of the ESCA MKII system of the new student surface laboratory"*

Abstract:

The Institute of Physics at NTNU are setting up a surface science student laboratory with a VG ESCA MKII Spectrometer. Our task in this project was to test the X-ray gun and LEED unit of this system, which are instruments useful for doing surface analysis.

We tested the X-ray gun, VGX, by using it to do XPS analysis of an Ag sample and comparing its results with that of a newer model X-ray gun, XR-50. To find out whether it was still functioning properly, we analysed and compared the flux of X-rays of the two X-ray guns, as well as checking to see whether or not the anode had been oxidised by looking at the low kinetic energy region of the spectrum from the VGX. The LEED unit was tested by using it to analyse a MoS2 sample and analysing its diffraction patterns to see whether or not it was distorted by stray fields affecting the path of electrons from the electron beam.

From our results, it seems both sets of equipment are functional and didn't have any specific problems that affected the results of the tests performed.

CONTENT

1. Introduction

The Institute of Physics at NTNU is currently in the process of establishing a new surface science student laboratory. For that a VG ESCA MKII Spectrometer was moved from the Electronics department to the new lab in the Natural Science Building. The equipment, however, is from 1987 and hasn't been used in the past ten years, so the different components need thorough testing to see if they are functioning properly.

In this project we tested the X-ray gun and the LEED unit of the ESCA MKII, which are both important components relevant to surface analysis of materials. As they are quite old, the VGX needed to be tested to see whether the anodes had been oxidised and if the intensity was still sufficient for XPS analysis, whereas the LEED unit needed to be tested to see if the path of electrons from the electron beam was being distorted by any stray fields.

1.1 Motivation

Our main motivation for participating in this project was to be part of the building of the new student laboratory and the possibility of continuing to be involved in running the student lab at a later time. Taking part in this project also allowed us to get hands-on experience with the equipment of the ESCA MKII, as well as deepen our knowledge regarding XPS and LEED analysis and equipment.

1.2 Acknowledgements

We would like to express our gratitude to the team working at the XPS lab, mainly Simon Cooil and Leander Michels, for their long hours and helpful demeanour.

2. Theory

2.1 X-ray spectroscopy (XPS) theory

XPS is a technique that allows us to look at the elemental composition of a surface. With XPS one intends to investigate the surface of a sample by ionizing it and measuring the energy of the photoelectrons ejected by the material after being exposed to an X-ray source[1]. This source often consists of either Aluminium (Al), Magnesium (Mg) or both, and it has a photon energy hv (Al and Mg have a K-alpha 1 energy of 1486 eV and 1253eV respectively).

These X-rays excite electrons to be ejected from either a valence or inner core shell (for example the 3d orbital). The two most common types of emitted electrons are photoelectrons and Auger electrons. Photoelectrons are emitted by being excited to a higher state after absorbing the photon energy, while Auger electrons are emitted as the material's electronic structure tries to reach a new equi-librium after a hole has been left by an emitted photoelectron[2]. The excited electrons have a very short mean free path inside the material, which is why only electrons from the surface of the sample (1-10nm deep) are emitted.

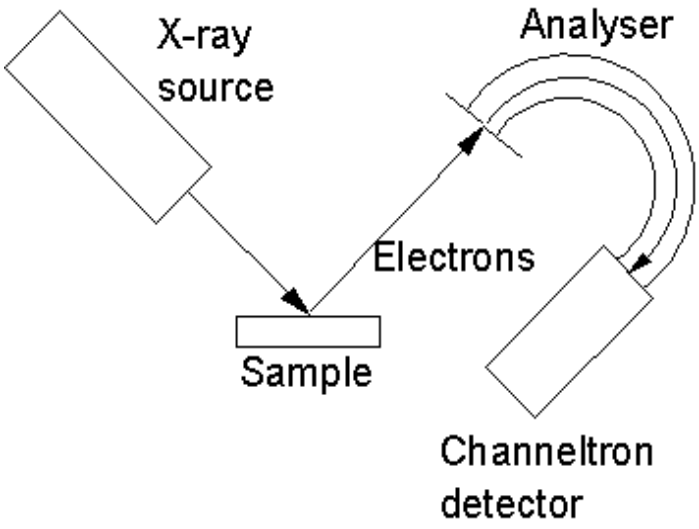

Figure 1: shows a schematic diagram of XPS apparatus (Petherbridge, 2002)

The energy of an ejected photoelectron is given by the photoelectric effect

$$E_{kin} = h\nu - E_{bin} - \Phi_A,$$

where E_{kin} is the kinetic energy for the photoelectron, $h\nu$ is the photon energy, E_{bin} is the binding energy (ground state) for the photoelectron and Φ_A is the work function of the analyser[2].

From this equation, we calculate the binding energy, from which we find the atom the electron comes from, as well as its chemical state.

2.1.1 XPS peak fitting theory and inverse square law

The aim of curve fitting is to estimate the parameter values that describe the set of data best[3]. With regards to XPS peak fitting there is an increase in counts as a function of kinetic energy when there is an excitation of core level electrons. We get information about the surface from these peaks. But before receiving the information, a peak fit must be done.

The Voigt approximation, which is a convolution of the Lorentzian and Gaussian functions, is used to characterize the area, position and FWHM[4]. Both are needed to make an adequate XPS peak fit.

In the XPS-fit we also need to remove the background signal to make a fit that only takes the relevant values (meaning the peaks) into consideration. In this report, we continuously used

the Shirley background subtraction in the simulation. The Shirley is an iterative determination of a background by using the areas labelled A1 and A2 (in the figure below) to get background intensity S as a function of energy E given by the equation[5]:

$$S(E) = I_2 + (I_1 - I_2) * \frac{A2(E)}{\left(A1(E) + A2(E)\right)}$$

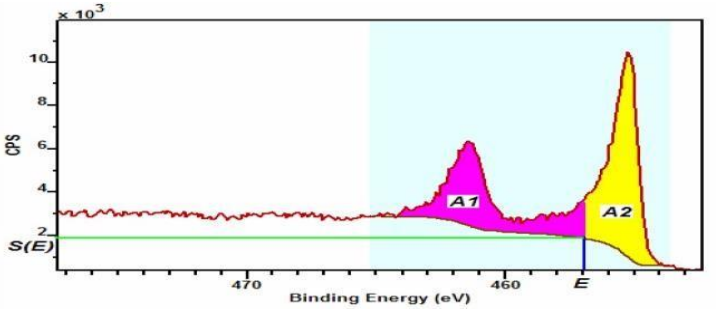

Figure 2: A graph that shows a background computed from a Ti 2p spectrum. (CasaXPS, 2006)

Full width at half maximum (FWHM) is another term for the width of the Voigt profile. The Voigt width is found by finding the Gaussian and Lorentzian widths by equations below:

(1) $f_G = 2\sigma * (2\ln(2))^{\frac{1}{2}}$ and (2) $f_L = 2\gamma$, where $\sigma = standard\ deviation.$

From these two function we put ϕ = (2)/(1) and get the equation for FWHM of the Voigt.

$$f_V = f_G\,(1 - C_0C_1 + \sqrt{\phi^2 + 2C_1\phi + C_0^2C_1^2}\,), where\ C_0 = 2{,}0056\ and\ C_1 = 1{,}0593$$

The spin orbit coupling and peak area ratio is defined by quantum mechanics and cannot change whether the element is in its pure or compound form (like in an alloy).

From literature, we have several theoretical values that we should expect. Spin orbit splitting for silver (Ag) is 6,0 eV[6]. Peak area ratio between Ag 3d (3/2) and Ag 3d (5/2) is found by:

L-S coupling is given by j = l +s, where l = angular momentum quantum number and s = spin angular momentum number and numerical values of $^{+}_{-}$1/2. The multiplicity of stats is given by 2j + 1 and this leads to the peak ratio being 2/3 for the two peaks. But it can vary slightly due to the background. The Shirley does not always take away all the background signals. Based on the theory, we can also expect the FHMW to be the same for both peaks.

When we compare the intensity of the two X-ray guns, we use the inverse square law equation:

$$\frac{I_1}{I_2} = \frac{D_2^2}{D_1^2}$$

2.2 Low energy electron diffraction (LEED) theory

Low energy electron diffraction (LEED) is a technique where a beam of low-energy electrons (~100eV) from an electron gun are sent at a sample, which leads to diffraction of electrons by the Bragg planes of the sample. Since the electrons have low energy, their mean free path is limited to the first few atomic layers[7]. This is why LEED and XPS are complementary methods of surface analysis; LEED gives an average of the reciprocal space of the surface structure while XPS gives an average of the chemical state of the surface.

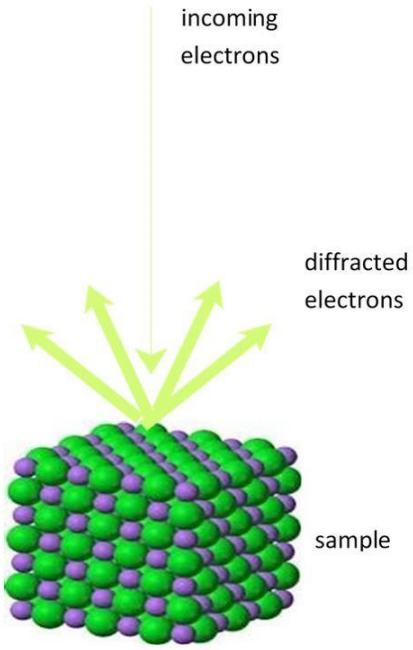

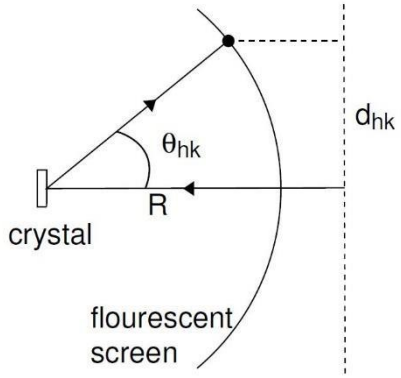

Figure 3: showcasing how the LEED instrument works (Hofmann, 2004)

Figure 4: Linear imaging of the reciprocal lattice by LEED (Hofmann, 2004)

The relation between the distance between the diffraction spots (the positions of the intensity maxima), d_{hk}, and the energy of the electron beam, E, can be seen in this equation[7]:

$$d_{hk} = R\sin\Theta_{hk} = \frac{R}{|\vec{k}|}(h\vec{g}_1 + k\vec{g}_2) = R\sqrt{\frac{\hbar^2}{2m}}\frac{1}{E^{1/2}}(h\vec{g}_1 + k\vec{g}_2).$$

From this equation, we get the relation

$$d_{hk} = \frac{x}{\sqrt{E}}$$

where x is a constant (as E is the only variable that is changed).

3. How the equipment works and the setup

In this part, we will show some basic explanation of the different components of the equipment as well as images of it.

3.1 Our samples

We had two samples we used to test the equipment in our project. One was for the XPS and the sample was a standard silver foil (Ag). The silver was polycrystalline and it is quite common to use silver to test out XPS equipment.

For LEED, we used molybdenum disulphide (MoS2), a semiconductor. It is a relatively unreactive compound at the bulk level, but very reactive at the surface, which makes it important to clean the sample surface before analysing it. MoS2 has a layered hexagonal structure (similar to graphite), which makes it suitable for LEED analysis.

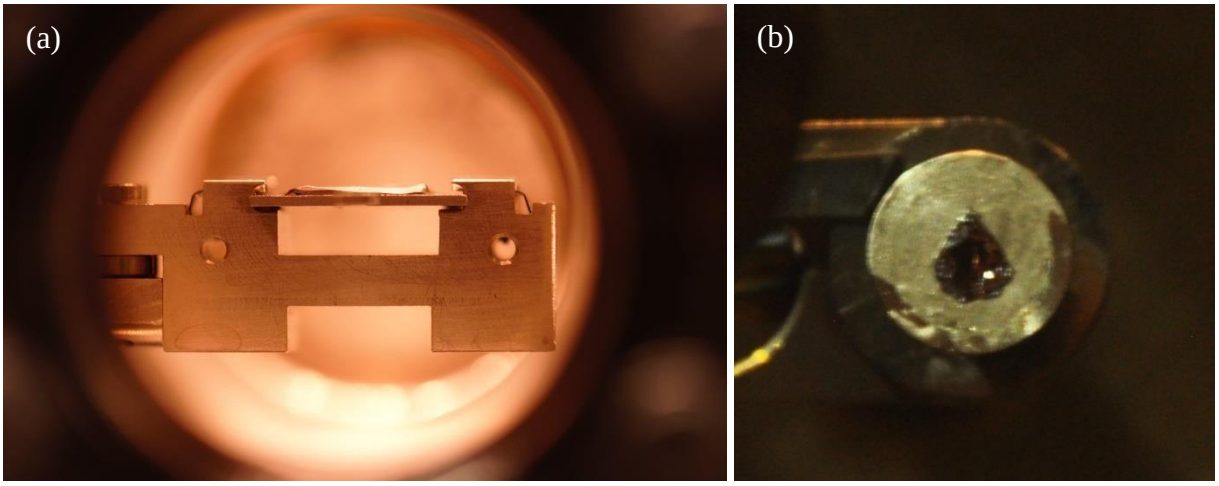

*Figure 5: Pictures of the samples. **(a)** is the mounted Ag foil, seen from the side, and **(b)** is the MoS2 glued to a sample holder.*

3.2 XPS equipment

In order to test and compare the X-ray guns, we attached the VGX to the UHV-chamber of the XPS lab with the XR-50 (UHV is necessary to get a long mean free path for the electrons after they have been ejected from the sample surface). The reason we attached them both to the same chamber is because we knew the electron analyser of this system was working, (while the one of the ESCA MKII had not been tested yet). It was also practical to only have to prepare and mount the sample once, in one chamber.

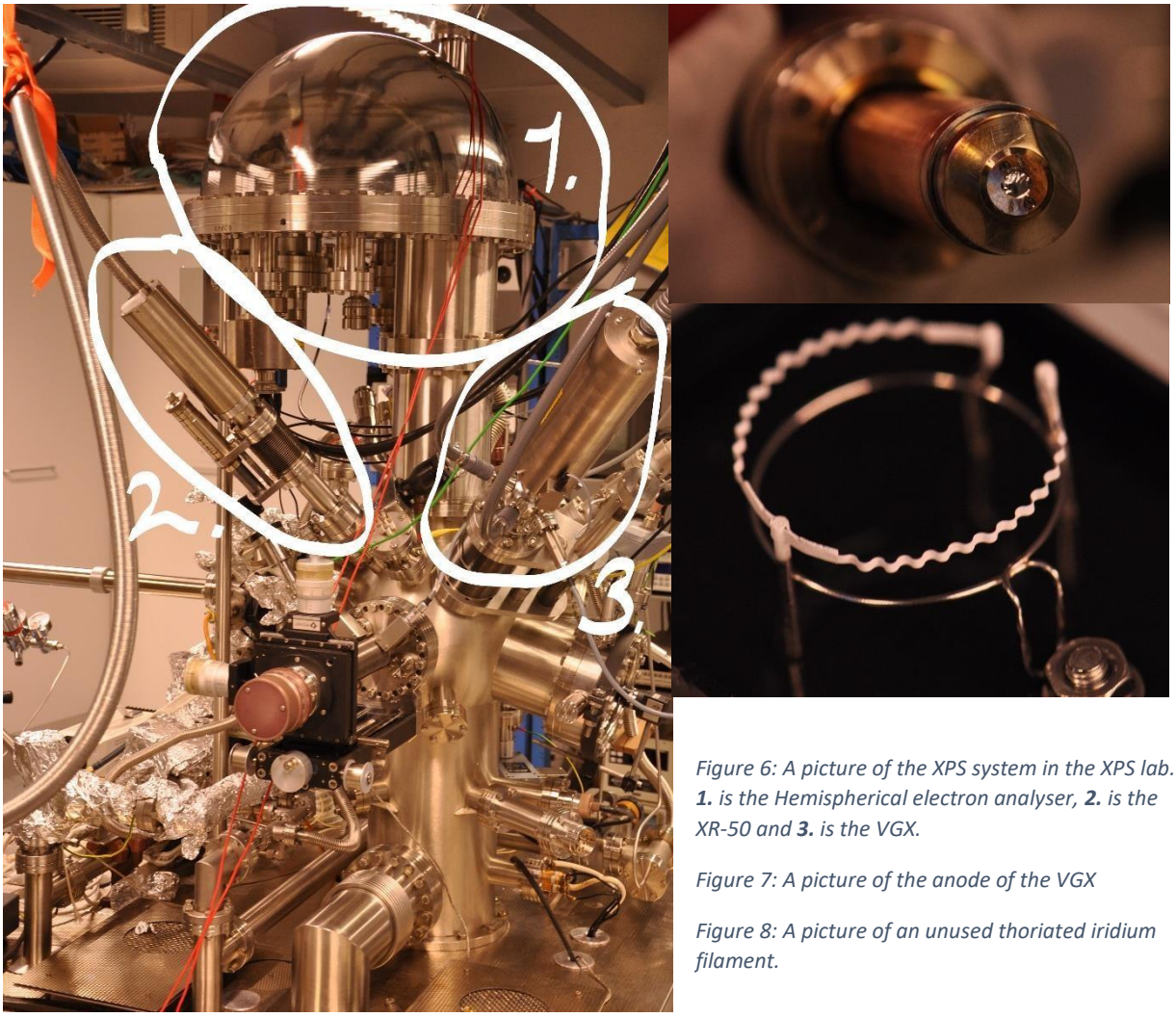

*Figure 6: A picture of the XPS system in the XPS lab. **1.** is the Hemispherical electron analyser, **2.** is the XR-50 and **3.** is the VGX.*

Figure 7: A picture of the anode of the VGX

Figure 8: A picture of an unused thoriated iridium filament.

The X-ray guns we used, the VGX of the ESCA MKII and the XR-50 of the XPS lab, were both Twin Anode X-ray Sources. As the name implies, Twin Anode X-ray Sources have two anodes, which is useful in that we get anodes with different photon energies as this shifts the kinetic energy of the photoelectron peaks, while the Auger peaks remain the same, as the Auger electrons are independent of the photon energy. Both X-ray guns had an Al and a Mg anode each, but we decided to only test the Al-anode of both.

To generate X-rays, thoriated iridium filaments are heated to emit electrons, which are attracted to high voltage running through the anode and accelerated onto it. As the electrons hit the anode, X-rays are emitted. To keep the anodes from getting too hot, there is a water cooling system inside the X-ray gun, and in the XR-50 the HV is even applied through the water. To allow for

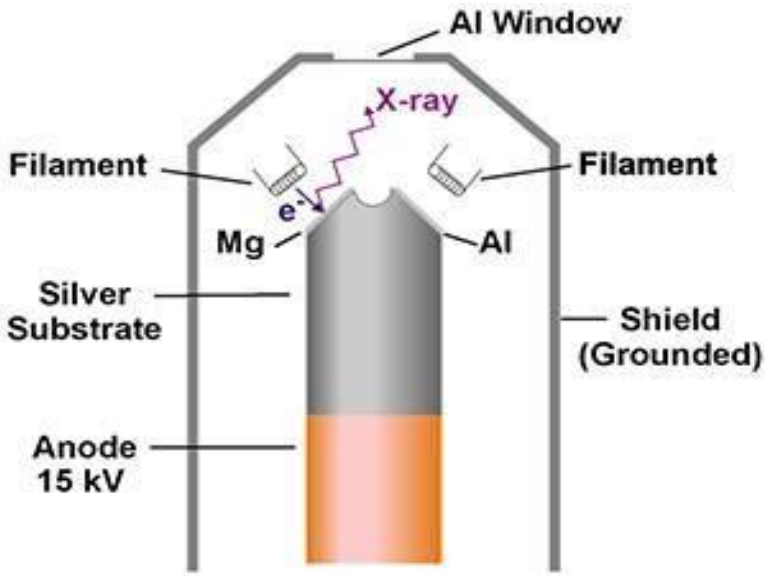

Figure 9: Shows anode and filament assembly of a Twin Anode X-ray source (Thermo Fisher Scientific Inc, n.d.)

the X-ray gun to be differentially pumped from the vacuum chamber, there is a housing made of Cu foil around it. The housing has a small Al window at the top which the X-rays can pass through. The housing also protects the anodes from contamination[8].

The electron analyser we used in the XPS lab was a hemispherical electron analyser.

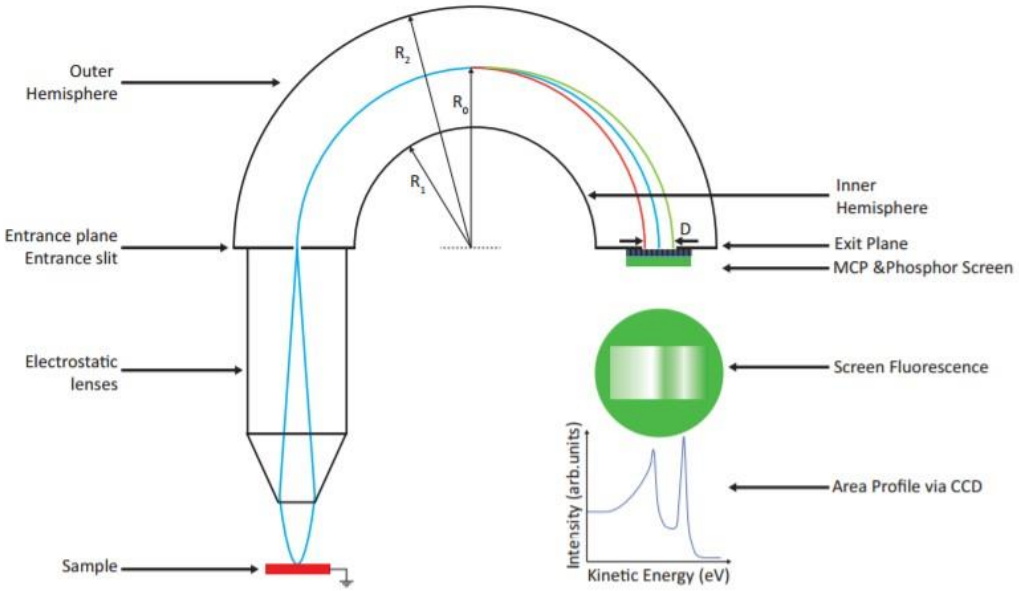

Figure 10: Shows the operating principles of a hemispherical electron analyser (Cooil, 2014).

The electrons emitted from the sample are attracted and focused by electrostatic lenses toward the entrance plane of the analyser. The electron analyser has two concentric hemispheres with two negative potentials applied between them. When the electrons enter, the electrostatic field caused by these potentials will cause the trajectories to bend. The pass energy of the system is the energy of the electrons that follow a circular trajectory and are able to reach the exit plane (if the energy is either too high or too low, the electron will collide with the walls of the hemispheres). At the exit plane the electrons pass through a slit, which can be adjusted in order to choose between electron count and higher resolution. The electrons that pass through are

then amplified by a Microchannel plate detector and hit a phosphorous plate with HV running through it, causing it to light up in areas hit by electrons. This can then be imaged by a CCD and converted into an area profile, resulting in a spectrum of kinetic energy as a function of the intensity[2].

3.3 LEED equipment

Regarding the LEED equipment, it consists of these main components: the electron gun, the detector and the mechanical turbomolecular vacuum pump. The turbomolecular pump is a combination of fixed and rotating blades that give the molecules direction and momentum. From the blades a high throughput and compression is acquired[9].

One of our tasks in the instrumentation part was to find out what kind of equipment the LEED instruments consisted of. The producer was Vacuum Generators (VG) from East Grinstead, England. It uses a model 640 Retarding Field Analyser, and is a standard four grid, front view LEED instrument[10]. Front view means that the electrons ejected from the sample are bounced back to a fluorescent screen which lights up, showing the diffraction pattern behind the sample.

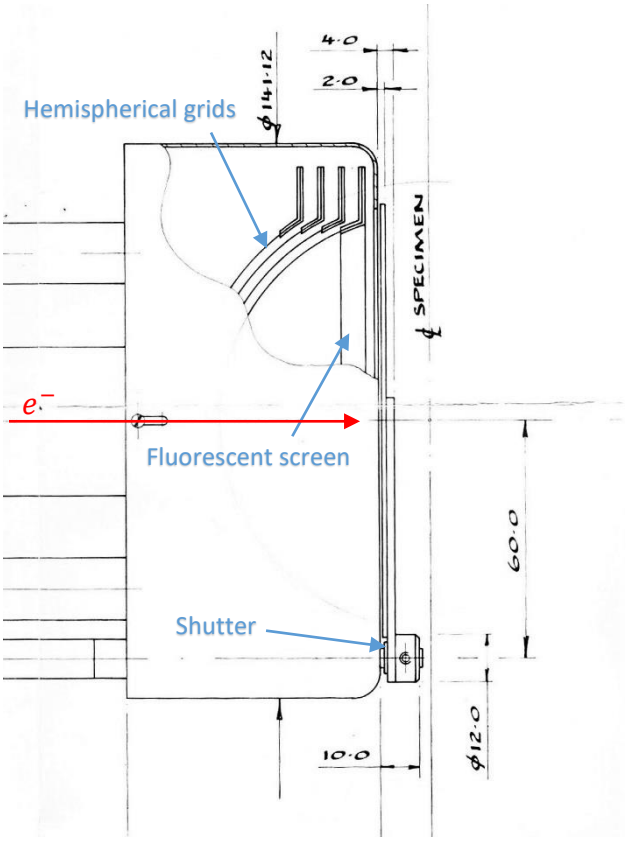

Figure 11: Schematics of part of the model 640 Retarding Field Analyser with a closed shutter (VG Scientific LTD, 1987)

Figure 12: is a picture of the model 640 Retarding Field Analyser (VG Scientific Limited, n.d.)

The LEED equipment also consisted of an LEG22 electron gun and a SPECS PH01BOS150 detector. The diffraction pattern on the detector could be directly viewed through a window in the wall of the vacuum chamber, and the pattern was recorded using a DSLR camera on a tripod.

4. Experimental

The execution of the project was divided in two parts; Comparing the two X-ray guns (XR-50 and VGX) through XPS analysis and testing the LEED unit of the ESCA MKII.

For the XPS analysis, the Ag sample was placed inside the vacuum chamber and sputtered with Argon (Ar) from an ion gun, in order to clean the surface. A single element surface was desired in order for the FWHM to be as narrow as possible.

During the sputtering, the pressure in the chamber increased to the $10^{-6}Pa$ level. After the sputtering was complete, the pressure went down to 10^{-9} - 10^{-10} Pa again.

In order to compare the two X-ray guns, we compared the linewidths and spectra we got from them. The X-ray guns were positioned at different distances from the sample, as illustrated in the figure below.

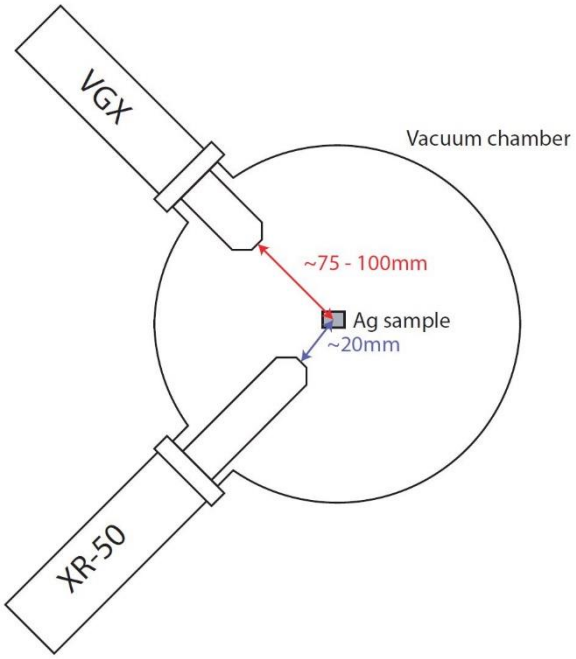

Figure 13: Illustrates the approximate distances between the X-ray guns and the sample in the vacuum chamber (Cooil, 2016)

The X-ray guns were both run at 20mA emission current and 13,5kV, in order for us to be able to compare the flux of X-rays. We scanned the kinetic energy area of the Ag peaks in order to compare the intensities of the X-ray guns. We also did a scan of the low kinetic energy region to see if the Al anode of the VGX had been contaminated with oxygen. For the XPS peak fitting, we used the data analysis and graphing software Origin.

In order to test the LEED unit, it was installed in the vacuum chamber of the ESCA MKII system. The MoS2 sample was prepared by cleaving it with scotch tape to remove the top layers of the surface together

with surface contaminants, in order to get a clean crystal structure before inserting it into the UHV. We photographed the diffraction patterns from two different electron beam energies, 97eV and 206eV, in order to compare them to check whether there were any stray fields distorting the path of the electron beam. The image analysis software Image J was used to analyse the patterns by enhancing the images and finding the distance between the diffraction spots.

5. Results and discussion

5.1 XPS results

We did 5 runs for both X-ray guns. Both spectra are an average of 5 sweeps in order to minimize signal to noise ratio.

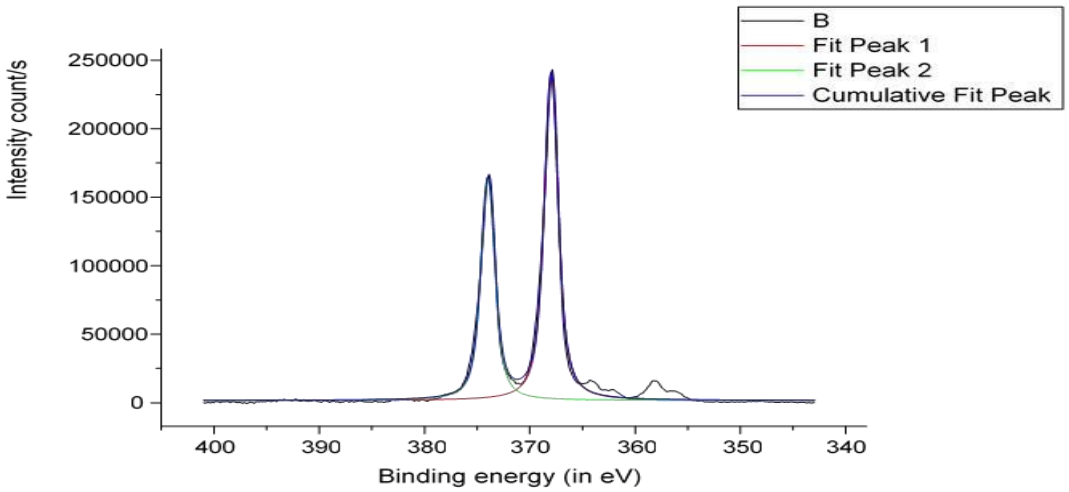

Figure 14: An average of VGX 3d orbital

We see slight peaks that the Shirley was not able to remove. They influenced the peak area ratio and are satellite peaks (photoelectron peaks), which means that they aren't background signal.

Material and orbit	Ag 3d (3/2)	Ag 3d (5/2)
Binding energy (in eV)	374	368
Peak (intensity count)	349741	523517
FWHM	1,62131	1,59409

Table 1: a table over the results from the VGX sample run

From figure 15, we can see that the spin orbit split is at 6 eV and that the peak intensity is (349741)/(523517) = 2/3. Both values are aligned with our expected values. Furthermore,

integrating the area from peak to peak (368 eV to 374 eV) gave us the area = 419868, 43 and the FWHM = 1,62.

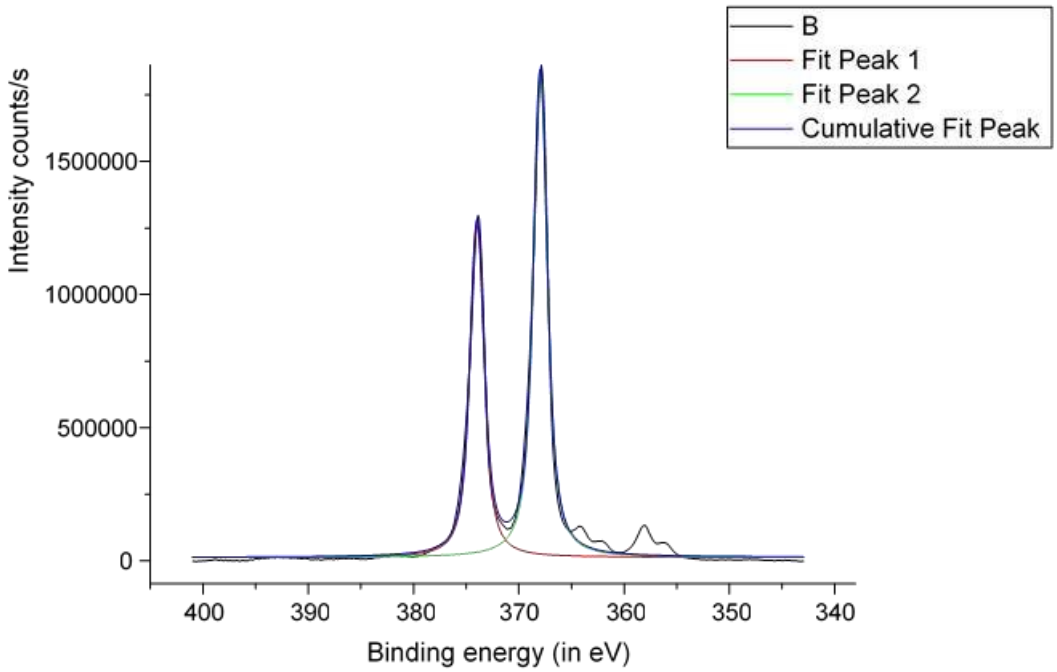

Figure 15: shows XR-50 run on Ag 3d

The second graph is of the XR-50. We see a higher intensity counts, but similar binding energy.

Material and orbit	Ag 3d (3/2)	Ag 3d (5/2)
Binding energy (in eV)	373,9	367,9
Peak (intensity counts)	2,793e6	4,102e6
FWHM	1,62057	1,60344

Table 2: shows the values we received from XR-50

We see again that the spin orbit splitting is at 6 eV, while the peak area ratio has changed a little bit to 68 %. It is still acceptable, but could have been lower. The reason this is the peak fitting that had to be done manually and the background subtraction. Background subtraction is the biggest source of error. The FWHM is roughly as for the VGX. An integration of the area from 367,9 to 373,9 lead to the value of: 3,34992e6 and a FWHM at 1,62.

The integration values can be used to find the proportion of intensity between the two X-ray guns and thereby compare them. From figure 13 in the experimental part we have the necessary values for D_1 and D_2

$$\frac{I_1}{I_2} = \frac{(20e-3)^2}{(75e-3)^2} = 0{,}07111$$

The intensity at 75mm for VGX is 419868,43. We must find I_2, the intensity of VGX at 20mm, in order to compare it with XR-50;

$$\frac{419868{,}43}{I_2} = 0{,}07111$$

$$I_2 = \frac{419868{,}43}{0{,}07111} = 5904492{,}055$$

Comparing I_2 with the intensity of XR-50, we get

$$\frac{5904492{,}055}{3349920} = 1{,}763,$$

indicating that the VGX has a higher flux of X-rays than the XR-50.

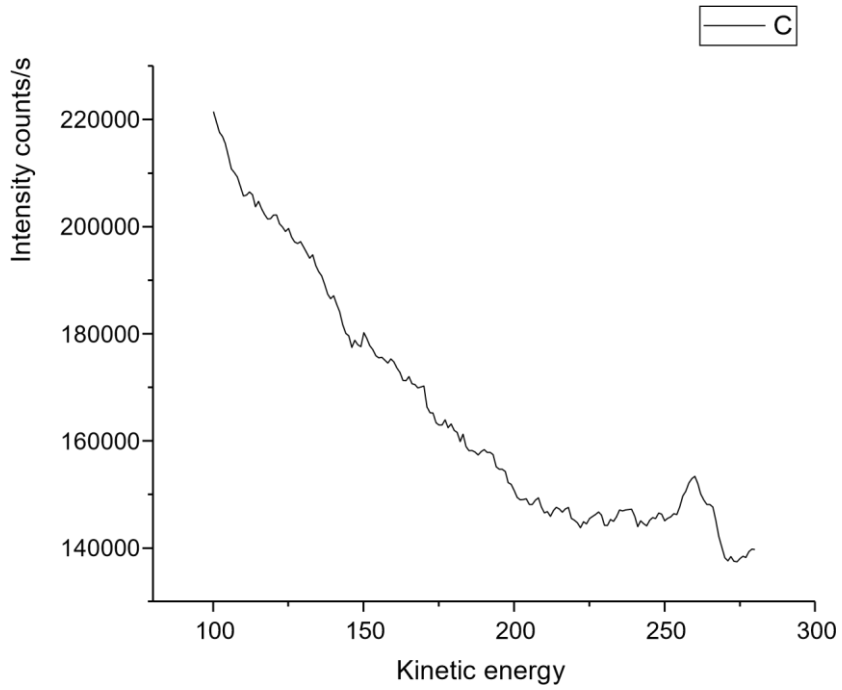

Figure 16: shows low kinetic energy region of the spectrum from VGX

Figure 16 shows a graph called the low kinetic energy region of the spectrum for VGX, which is supposed to show if there is any oxygen contamination on the X-ray gun. We make use of the equation: $E_{kin} = h\nu - E_{bin} - \Phi_A$. This gives us,

$$E_{kin} = 525\ eV - 368\ eV - 4{,}3\ eV = 152{,}7\ \text{eV}$$

for the Ag 3d[11]. That means that if there is any oxygen on the gun, then there should be a peak at 152,7 eV.

We can see from figure 15 that this is not the case and which leads us to believe that there is very little oxygen on the VGX.
We look at the XR-50 as well.

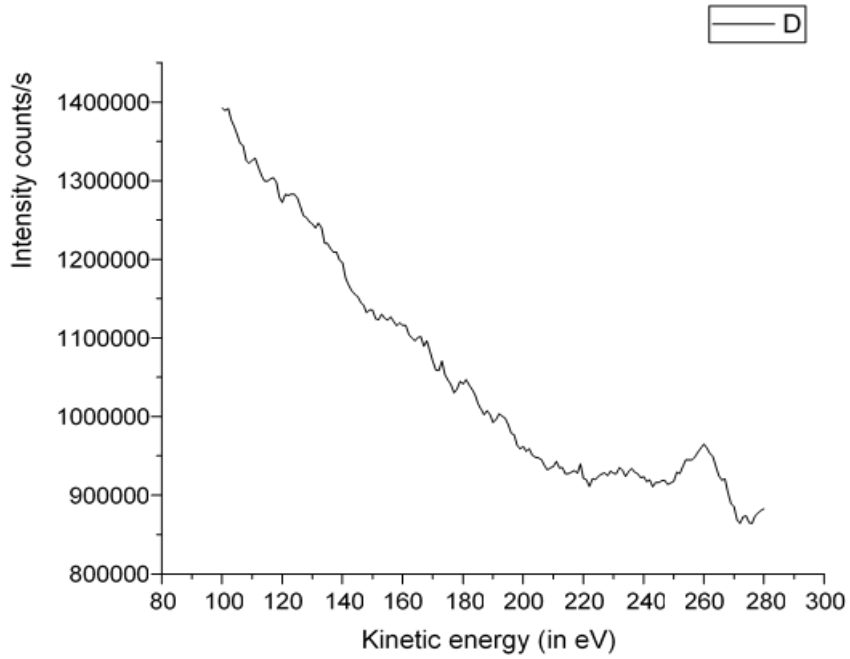

Figure 17: shows the low kinetic energy region of the spectrum from XR-50

We can see from that the resonation from above is valid in this case too.

The last part we evaluated was the detector. Electrostatic field within the detector only allow electrons of a certain energy pass into the detectors slit. The value for our low pass energy system was 30 eV or lower.

5.2 LEED results

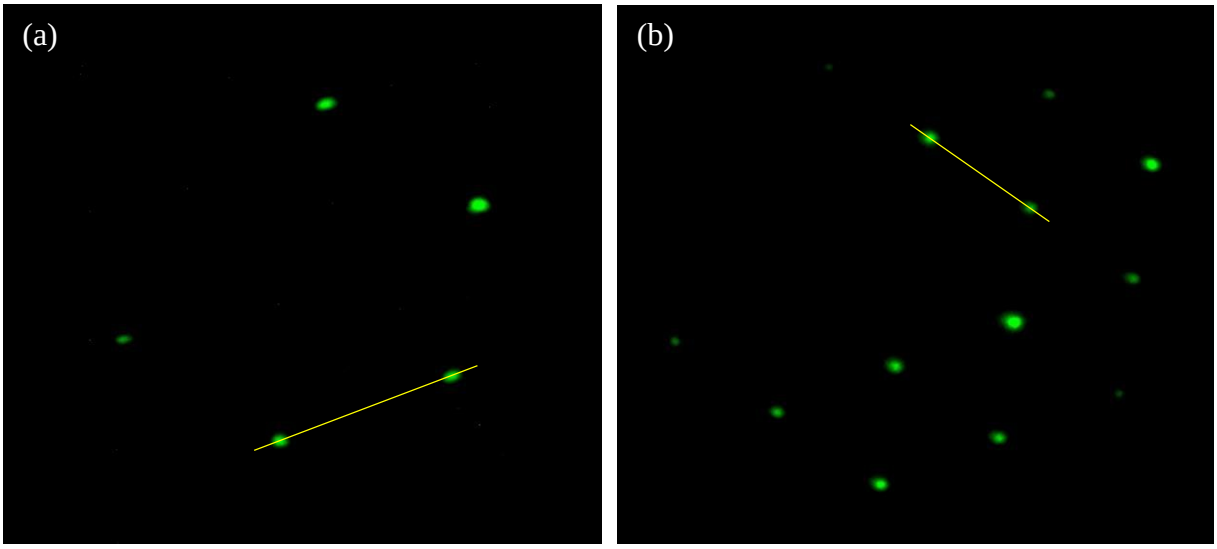

*Figure 18: LEED patterns of a MoS2 sample, **(a)** is with an electron beam energy 97eV and **(b)** is with 206eV. The yellow lines show how the distance between the diffraction spots was measured.*

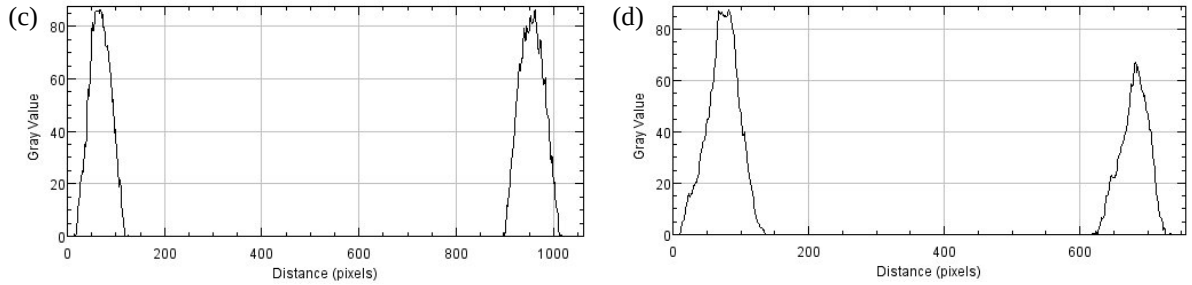

*Figure 19: **(c)** shows the distance between the diffraction spots marked by the yellow line on the 97eV pattern in pixels. The peaks represent the middle of the spots. **(d)** similarly shows the distance between the spots of the 206eV pattern.*

We got clear LEED patterns from the MoS2 sample, and the patterns above are from the electron beam energies $E_1 = 97eV$ and $E_2 = 206eV$. The patterns clearly show the hexagonal pattern expected of the sample. In order to test the performance of the LEED equipment, we decided to see whether the ratio between the distance between the spots scaled in accordance with the change in energy. From the equation of the relation between the energy and the distance, $d_{hk} = \frac{x}{\sqrt{E}}$ we can derivate:

$$d_{hk1} = \frac{x}{\sqrt{E_1}}, \quad d_{hk2} = \frac{x}{\sqrt{E_2}}, \quad E_2 = \frac{206}{97} E_1$$

$$d_{hk2} = \frac{x}{\sqrt{\frac{206}{97} E_1}} = \frac{d_{hk1}}{\sqrt{\frac{206}{97}}}$$

$$\frac{d_{hk1}}{d_{hk2}} = \sqrt{\frac{206}{97}} \approx 1{,}46$$

To measure the distance between the spots on the diffraction patterns we got using the LEED, we used the program Image J. The method used was drawing straight lines between the centres of the spots closest to each other and measuring the distance in pixels, as shown in figure 18 and 19 above. For the energies E_1 and E_2, we measured the distances $d_1 = 890\ pixels$ and $d_2 = 605\ pixels$.

$$\frac{d_{hk1}}{d_{hk2}} = \frac{d_1}{d_2} = \frac{890}{605} \approx 1{,}47.$$

6. Conclusion

Our project was varied and very interesting. We managed to educate ourselves on both XPS and LEED instruments, while at the same time increasing our software skills with the programs Origin and Image J.

With regards to XPS results we found that Ag 3d has binding energy at 368 eV and 374 eV. We also found that the intensity of VGX gun was roughly 1,763 times that of the XR-50 when adjusted to the distance. There was no oxygen contamination on the anode based on the secondary electron (tail) measurements.

As for testing the LEED equipment we got a clear diffraction pattern, and the measured ratio of 1,47 was very close to the theoretical 1,46. The most likely cause of inaccuracies in this case (where the sample was good) would be the means of measuring the distance between the spots by drawing a line between them. Another possible cause is that the pattern was recorded using a camera on a tripod, and the pattern would be elongated if the camera wasn't pointed perpendicularly at the detector. However, from the measurements we took we cannot detect any noticeable distortion of the electron path.

From these results we believe both the VGX and the LEED equipment of the ESCA MKII are still functioning and ready for use in the student lab. The next step of preparing the equipment would be to test the hemispherical electron analyser of the ESCA MKII, installing the equipment on the vacuum chamber and checking that there aren't any leaks. We look forward to the time when the equipment is all installed and the surface science student laboratory is ready for use.

7. Work distribution

Both of us took part in all experiments in this project. Furkan did the XPS peak fitting and results, while Gina did the LEED analysis. Furkan wrote the parts XPS peak fitting theory and XPS results. Gina wrote X-ray spectroscopy (XPS) theory, XPS equipment and LEED results. The rest was written in cooperation by both. The photographs used in this report were all taken by Gina.

8. References

1. Leng, Y., *Material characterization.* Wiley, 2003. p. 47
2. Cooil, S.P., *Controlling the epitaxial growth of graphene on diamond surfaces.* Thesis submitted to Aberystwyth University, 2014.
3. OriginLab. *15.5.3 Theory of nonlinear curve fitting*. 2016; Retrieved from: http://originlab.com/doc/Origin-Help/NLFit-Theory (Accessed 5th Dec 2016)
4. CasaXPS. *Help manual and Line Shapes.* 2005; Retrieved from: http://www.casaxps.com/help_manual/line_shapes.htm
5. CasaXPS. *Peak fitting in XPS.* 2006; Retrieved from: http://www.casaxps.com/help_manual/manual_updates/peak_fitting_in_xps.pdf
6. Biesinger, M.C., *Spin orbit splitting.* 2015; Retrieved from: http://www.xpsfitting.com/search/label/Spin%20Orbit%20Splitting (Accessed 5th Dec 2016)
7. Hofmann, P., *Lecture notes on Surface Science*, Aarhus University, 2004. p. 82-97
8. Thermo Fisher Scientific Inc., *Twin anode X-ray Sources*, n.d.; Retrieved from: http://xpssimplified.com/xray_generation.php (Accessed 10th Dec 2016)
9. Quirk, M. and Serda, J., *Semiconductor Manufacturing Technology.* Pearson Education, 2000
10. VG Scientific Limited, *Features of the model 640 RFA*, East Grinstead, n.d.
11. Harvard University., *X-ray emission lines.* 2016; Retrieved from: http://www.med.harvard.edu/jpnm/physics/refs/xrayemis.html (Accessed 5th Dec 2016)
12. Cooil, S.P., *Setup of X-ray guns* [image], NTNU, 12th Dec 2016
13. VG Scientific LTD, *640- Retarding Field Analyser* [blueprint], East Grinstead, 1987
14. Petherbridge, J.R., *Figure 2.5 Schematic diagram of XPS apparatus* [image], University of Bristol, 2002, Retrieved from: http://www.chm.bris.ac.uk/pt/diamond/jamespthesis/chapter2.htm (Accessed 21. Dec 2016)